JOURNAL OF THERMOPHYSICS AND HEAT TRANSFER
Vol. 8, No. 3, July–Sept. 1994

Finite Element Formulation of the Discrete-Ordinates Method for Multidimensional Geometries

W. A. Fiveland* and J. P. Jessee†
Babcock & Wilcox Company, Alliance, Ohio 44601

Radiative heat transfer in a multidimensional participating medium was predicted using the discrete-ordinates (DO) method. The even parity radiative transfer equation (RTE) is formulated for an absorbing, isotropically scattering, and re-emitting medium enclosed by gray walls. The even parity RTE is spatially discretized with the finite element method. The solution accuracy and convergence are discussed for several element types. Several test enclosures are modeled. Results are compared with the standard DO control volume formulation, exact solutions, and the P_3 differential approximation. Solutions are found for enclosures with either absorbing or isotropically scattering media. Results compare well with published results. Also, the use of the method for complex geometries and unstructured grids is discussed.

Nomenclature

E_b = emissive power, $\bar{\sigma}T^4$, W/m^2
G = incident energy, $\int_{4\pi} I\, d\Omega$, W/m^2
G^* = nondimensional incident energy, G/E_b
I = intensity, $I(\bar{r}, \bar{\Omega})$, W/m^2·sr
L = characteristic length, m
M = total number of discrete ordinate directions
N = total number of global nodes
N_i = basis function
n = surface normal
Q^* = nondimensional net wall heat flux, q/E_b
q = heat flux, $\int_{2\pi} |\hat{n}\cdot\bar{\Omega}| I\, d\Omega$, W/m^2
r = position vector, m
S_m = in-scattering source term, W/m^3-sr
S_n = order of discrete ordinates approximation
w = weight function
w_m = direction weights
x, y, z = coordinate directions, m
x^*, y^*, z^* = nondimensional coordinates, x/L, y/L, z/L
α = nonuniform mesh parameter
β = extinction coefficient, m^{-1}
Γ = boundary of domain, Λ
ε = emissivity
κ = absorption coefficient, m^{-1}
Λ = domain
μ, ξ, η = direction cosines
ρ = reflectivity, $1 - \varepsilon$
$\bar{\sigma}$ = Boltzmann's constant, W m^{-2} K^{-4}
σ = scattering coefficient, m^{-1}
ϕ = net intensity, W/m^2-sr
Ψ = average intensity, W/m^2-sr
$\bar{\Omega}$ = direction with direction cosines, μ, ξ, η

Subscripts

b = blackbody
m = direction
n = nth S_n approximation

Superscripts

$'$ = incoming direction
$*$ = nondimensional value
$\bar{\ }$ = vectorial quantity
$\hat{\ }$ = unit vector

Introduction

IN many high-temperature applications including combustion in furnaces and industrial and utility boilers, radiation heat transfer with a participating media is the dominant mode of heat transfer. Consequently, the proper characterization of these processes requires accurate radiation heat transfer methods.

There has been recent interest in developing radiation heat transfer methods applicable to multidimensional geometries. Monte Carlo methods,[1] zonal methods,[2,3] and approximate methods[4,5] have been developed for multidimensional geometries. Monte Carlo and zonal methods are too time-consuming and tedious to apply for scattering problems. Approximate methods are often developed for selective cases of radiative heat transfer and are not robust computational methods. Consequently, alternate schemes of radiative heat transfer are required for practical application. They have been extensively reviewed elsewhere.[6] Of these methods, the discrete ordinates method has received considerable attention, because it has several desirable features.[7–10] The method is relatively easy to code, requires a single formulation to invoke higher-order approximations, and the method integrates easily into control volume transport codes.

However, the discrete ordinates (DO) method is not without problems:

1) The standard discrete ordinate formulation may produce negative intensities, which are physically unrealistic. To achieve a realistic solution, many workers[7,8,11] have used "flux fix-ups" that range from zeroing the negative intensities to a positive intensity scheme. However, despite these artificial corrections, one sacrifices accuracy and computational speed.

2) Conventional formulations with the radiant intensity as the dependent variable are solved using an explicit streaming method on orthogonal, structured grids. Formulations to date have applied to rectangular geometries. Many practical geometries have irregular boundaries, and therefore, a general discretization method is desirable.

This article presents a novel formulation of the discrete ordinates method for radiative heat transfer applications using even-parity equations.[12] The formulation overcomes many problems associated with the conventional formulation, and facilitates the discretization of the governing equations with the finite element method (FEM). The application of the FEM permits the modeling of irregular boundaries, the continuous representation of spatially varying properties, the use of un-

Received April 12, 1993; revision received Nov. 5, 1993; accepted for publication Nov. 8, 1993.

*Supervisor, Heat Transfer & Fluid Mechanics Section, Research and Development Division. Member AIAA.

†Research Engineer, Heat Transfer & Fluid Mechanics Section, Research and Development Division.

structured grids, the implementation adaptive gridding (h or p methods), and the use of multigrid solution algorithms. In addition, the FEM formulation facilitates use of the DO method in FEM flow codes.

The equations are formulated for an absorbing, isotropically scattering, and re-emitting medium enclosed by gray walls. The solution accuracy and convergence is discussed for 4- and 8-node elements. Several test enclosures are modeled. Results have been obtained for the S_2, S_4, S_6, and S_8 approximations.

Analysis

Governing Equations

Consider the radiative transfer equation for the region, Λ, shown in Fig. 1. The balance of energy passing in a specified direction $\vec{\Omega}$ through a small differential volume in the emitting-absorbing and isotropically scattering gray medium can be written as follows:

$$(\vec{\Omega}\cdot\nabla)I(\vec{r},\vec{\Omega}) = -(\kappa+\sigma)I(\vec{r},\vec{\Omega}) + \kappa I_b(\vec{r}) + \frac{\sigma}{4\pi}\int_{4\pi} I(\vec{r},\vec{\Omega}')\,d\Omega' \quad (1)$$

where $I(\vec{r},\vec{\Omega})$ is the radiation intensity, which is a function of position and direction; $I_b(\vec{r})$ is the intensity of blackbody radiation at the temperature of the medium; and κ and σ are the gray absorption and scattering coefficients of the medium, respectively.

If the surface Γ, bounding the region Λ, is assumed gray and emits and reflects diffusely, then the radiative boundary condition for Eq. (1) is given by

$$I(\vec{r},\vec{\Omega}) = \varepsilon I_b(\vec{r}) + \frac{\rho}{\pi}\int_{\hat{n}\cdot\vec{\Omega}'<0} |\hat{n}\cdot\vec{\Omega}'|I(\vec{r},\vec{\Omega}')\,d\Omega' \quad (2)$$

where $\vec{r}$ belongs to Γ and $\vec{\Omega}\cdot\hat{n} > 0$. $I(\vec{r},\vec{\Omega})$ is the intensity leaving a surface at a boundary condition location, ε is the surface emissivity, ρ is the surface reflectivity, and $\hat{n}$ is the unit normal vector at the boundary location.

The even parity form of the RTE is derived by considering opposing directions $\vec{\Omega}$ and $-\vec{\Omega}$, and by defining the following quantities:

$$\Psi(\vec{r},\vec{\Omega}) = \tfrac{1}{2}[I(\vec{r},\vec{\Omega}) + I(\vec{r},-\vec{\Omega})] \quad (3a)$$

$$\phi(\vec{r},\vec{\Omega}) = \tfrac{1}{2}[I(\vec{r},\vec{\Omega}) - I(\vec{r},-\vec{\Omega})] \quad (3b)$$

Equation (1) can be written for the directions $\vec{\Omega}$ and $-\vec{\Omega}$, respectively. Adding and subtracting the resulting equations using Eqs. (3a) and (3b) leads to the following:

$$\vec{\Omega}\cdot\nabla\phi(\vec{r},\vec{\Omega}) = -\beta\Psi(\vec{r},\vec{\Omega}) + (\sigma/4\pi)\int\Psi(\vec{r},\vec{\Omega}')\,d\Omega' + \kappa I_b(\vec{r}) \quad (4a)$$

$$\vec{\Omega}\cdot\nabla\Psi(\vec{r},\vec{\Omega}) = -\beta\phi(\vec{r},\vec{\Omega}) \quad (4b)$$

The corresponding form of the boundary conditions is

$$\Psi(\vec{r},\vec{\Omega}) + \phi(\vec{r},\vec{\Omega}) = \varepsilon I_b(\vec{r}) + (1-\varepsilon)[q'(\vec{r})/\pi] \quad (5a)$$

where $\vec{r}$ belongs to Γ, and Eq. (5a) applies for $\vec{\Omega}\cdot\hat{n} > 0$. A second boundary condition can be written

$$\Psi(\vec{r},\vec{\Omega}) - \phi(\vec{r},\vec{\Omega}) = \varepsilon I_b(\vec{r}) + (1-\varepsilon)[q'(\vec{r})/\pi] \quad (5b)$$

where $\vec{r}$ belongs to Γ and Eq. (5b) applies for $\vec{\Omega}\cdot\hat{n} < 0$.

A second-order form of the transport equation can be obtained by solving Eq. (4b) for ϕ, and eliminating ϕ from Eq. (4a)

$$-(\vec{\Omega}\cdot\nabla)(1/\beta)(\vec{\Omega}\cdot\nabla)\Psi(\vec{r},\vec{\Omega}) = -\beta\Psi(\vec{r},\vec{\Omega}) + (\sigma/4\pi)\int\Psi(\vec{r},\vec{\Omega}')\,d\Omega' + \kappa I_b \quad (6)$$

This equation is termed the "even parity equation."[12] It is a second-order equation that has been shown to be positive definite and self adjoint.[13] Boundary conditions are found by eliminating the ϕ from Eqs. (5a) and (5b) using Eq. (4b).

Discrete-Ordinate Equations

Equations (5a) and (5b) and Eq. (6) are replaced by a discrete set of equations for a finite number of directions, $\vec{\Omega}_m$, and each integral is replaced by a quadrature. The resulting discrete ordinate equations are

$$-(\vec{\Omega}_m\cdot\nabla)\frac{1}{\beta}(\vec{\Omega}_m\cdot\nabla)\Psi(\vec{r},\vec{\Omega}_m) = -\beta\Psi(\vec{r},\vec{\Omega}_m) + \frac{\sigma}{4\pi}\sum_{k=1}^{N_w} w_k\Psi(\vec{r},\vec{\Omega}_k) + \kappa I_b \quad (7)$$

where $\vec{\Omega}_m$ is the discrete direction, and w_k is the weight corresponding to the incoming direction $\vec{\Omega}_k$. For a Cartesian geometry, the operator is given as

$$\vec{\Omega}_m\cdot\nabla = \mu_m\frac{\partial}{\partial x} + \eta_m\frac{\partial}{\partial y} + \xi_m\frac{\partial}{\partial z} \quad (8)$$

where the values μ_m, η_m, and ξ_m are the direction cosines of $\vec{\Omega}_m$. The direction cosines and weights for the S_2, S_4, S_6, and S_8 (S_n) approximations are listed in Refs. 8 and 9.

Finite Element Method

The weighted residuals approach[14] is used to spatially discretize the discrete ordinate equations. The governing equation is weighted over the domain of interest and its integrated residuals are set to zero

$$\int_\Lambda w(\text{equation 7})\,d\Lambda = 0 \quad (9)$$

where w denotes all weighting functions in an infinite dimensional set. Equation (9) can be integrated by parts to obtain a "weak" form of the governing equation

$$\int_\Lambda \nabla\cdot w\vec{\Omega}\left(\frac{1}{\beta}\nabla\cdot\vec{\Omega}\Psi_m\right)d\Lambda - \int_\Lambda \nabla w\cdot\vec{\Omega}\left(\frac{1}{\beta}\nabla\cdot\vec{\Omega}\Psi_m\right)d\Lambda - \int_\Lambda w\beta\Psi_m\,d\Lambda + \int_\Lambda wS_m\,d\Lambda = 0 \quad (10)$$

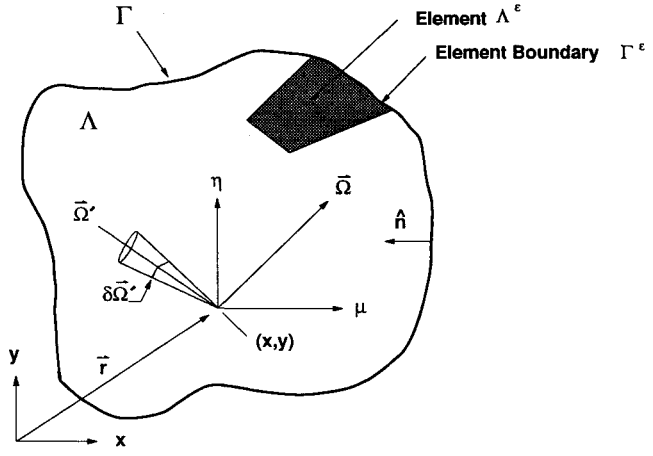

Fig. 1 Domain Λ and boundary Γ.

where $m = 1, \ldots, M$ are the discrete ordinate directions. The term S_m in Eq. (10) denotes sources from emission and in-scattering.

Application of Green's theorem may be used on the first term of Eq. (10) to obtain

$$\int_\Gamma w\vec{\Omega}\left(\frac{1}{\beta}\nabla\cdot\vec{\Omega}\Psi_m\right)\cdot\hat{n}\,d\Gamma - \int_\Lambda \nabla w\cdot\vec{\Omega}\left(\frac{1}{\beta}\nabla\cdot\vec{\Omega}\Psi_m\right)d\Lambda - \int w\beta\Psi_m\,d\Lambda + \int wS_m\,d\Lambda = 0 \quad (11)$$

The integration with Γ in Eq. (11) may be further simplified recognizing that the term in parentheses is ϕ defined in Eq. (4b) to obtain

$$\int_\Gamma w\phi_m|\vec{\Omega}\cdot\hat{n}|\,d\Gamma - \int_\Lambda \nabla w\cdot\vec{\Omega}\left(\frac{1}{\beta}\nabla\cdot\vec{\Omega}\Psi_m\right)d\Lambda - \int_\Lambda w\beta\Psi_m\,d\Lambda + \int_\Lambda wS_m\,d\Lambda = 0 \quad (12)$$

The domain of interest is subdivided and Eq. (12) is written for each element, see Fig. 1. Applying the Galerkin method and using isoparametric elements, the variation across each element is described with 4- or 8-node shape functions[15]

$$\vec{r} = \sum_j^N N_j\vec{r}_j \qquad \Psi_m = \sum_j^N N_j\Psi_{jm} \quad (13)$$

and the arbitrary weight function is restricted to the set of basis functions

$$w \in (N_i;\ i = 1, \ldots, N) \quad (14)$$

where N is the total number of nodes in the finite element mesh. Substituting Eqs. (13) and (14) into Eq. (12) provides N integral equations for each of the discrete ordinate directions. The integrals in these equations are approximated with Gaussian quadrature to provide a discrete set of algebraic equations. Integrals with $d\Lambda$ are reduced with a 9-point integration, and integrals with $d\Gamma$ are reduced with a 3-point integration. The matrix system of equations can be symbolically written

$$a_{ijm}\Psi_{jm} = S_{im} \quad \text{for} \quad m = 1, \ldots, M \quad (15)$$

Solution Methods

The discretized even parity form of the transport equation is represented by Eq. (15). In the present work, each m direction was solved independently. As a result, global iterations were necessary to include the source term and boundary conditions. With Ψ known for each direction, the incoming surface heat flux q' can be determined using Eqs. (3a), (3b), and (5a) or (5b), together with the definition of q'. The source term and wall heat fluxes were calculated based on the solution from the previous global iteration, and then a system of equations was solved for each ordinate direction. Global iterations continued until convergence was obtained. The formulation does not produce negative intensities, so flux fixups are not necessary.[7,8] A direct solver was used to solve the linear system of equations for each direction. Other solvers specifically designed for the banded matrices would speed calculations, but were not used in the present work.

In contrast to the above algorithm, the entire system of discretized equations [defined by Eq. (15)], in principle, could be solved using a linear equation solver since the problem is linear in Ψ. The in-scattering terms, of course, would have to be moved to the left side of Eq. (15) to provide the implicit dependence on Ψ. This approach eliminates the need for time-consuming global iterations, and greatly improves the coupling between directions. Consequently, such an approach becomes attractive when either large extinction coefficients or highly reflective surfaces are considered. The resulting "stiffness" matrix, a_{ijm}, is relatively sparse, and iterative linear equation solvers, such as those employing preconditioned conjugate gradient methods, would be more appropriate than direct solvers.

Results

The geometry studied in this article is a two-dimensional rectangular enclosure shown in Fig. 2, which is a special case of the geometry depicted in Fig. 1. Three cases are examined: 1) scattering medium in a black enclosure, 2) scattering medium in a gray enclosure, and 3) absorbing medium in a black enclosure. These examples were used to benchmark the even parity solutions against exact solutions, the standard DO (CV DOM) formulation with a diamond difference, the zone method, and P_3 approximations.

Solutions were found using the level symmetric S_n quadrature documented in several references.[9,16] Solutions were found using S_2, S_4, S_6, and S_8 approximations. Equations (5) and (7) require $\frac{1}{2}n(n+2)$ directions for a three-dimensional S_n analysis, and $\frac{1}{4}n(n+2)$ directions for a two-dimensional analysis. This is one-half the directions required by the standard control volume discrete-ordinate formulation using radiant intensity as the dependent variable.

The two-dimensional rectangular enclosure was subdivided into an even number of elements in each direction, i.e., 1×1, 2×2, $\ldots$, 10×10. Both 4- and 8-point elements were used. The wall emissivity and scattering and absorption coefficients were established for each case and were assumed not to vary. Convergence was measured using the change in the incident energy. Iterations were continued until the change in incident energy was less than 0.01%. For the cases considered, the balance between energy absorbed in the volume and the net flux matched to 7 digits. Results are presented using nondimensional values; net wall heat fluxes and radiant intensities are normalized using a characteristic emissive power, while coordinate directions are normalized with a characteristic length.

Pure Scattering in Black Enclosures

Radiative transfer in a square enclosure with black walls and an isotropically scattering medium was studied. This geometry has been analyzed before[4,7] and serves as a good benchmark for the finite element method. For the two-dimensional rectangular geometry, the lower wall ($y^* = 0$) has an emissive power of unity, and the other walls have zero emissive power. All walls are radiatively black, $\varepsilon = 1$. Ten to fifteen iterations were required to achieve converged so-

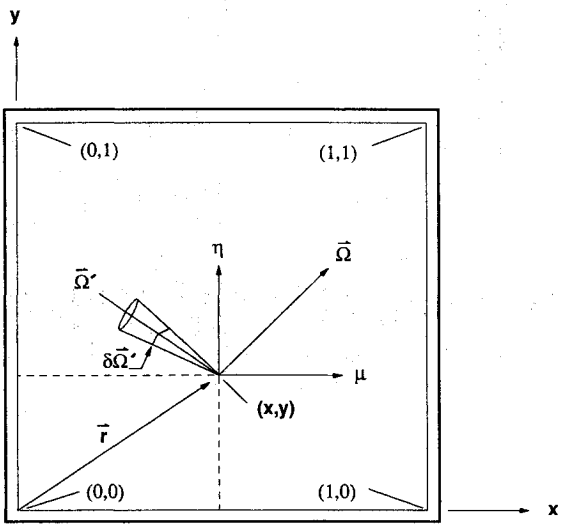

Fig. 2 Problem domain Λ and boundary Γ.

lutions for scattering in a black enclosure. Solutions are presented for 4-node elements. Figures 3 and 4 exhibit the net wall heat flux and incident energy for the finite element solutions.

Figure 3 shows the predicted net wall heat flux for several FEM solutions compared to the zone solution and the standard discrete ordinates method. The S_2 DO approximation significantly underpredicts the heat flux predicted by the zone method. In general, the errors for S_4 to S_8 are within 5%. The FEM S_6 and S_8 solutions compare better with the zone method than the FEM S_4 solution, but the higher approximations require more execution time. The FEM solutions for these conditions are not as accurate as the discrete ordinate formulation[7] using the quadrature from Ref. 9.

Figure 4 shows three profiles of incident energy at $x^* = 0.1$, 0.3, and 0.5. The finite element DO solutions for the S_4 and S_8 solutions are compared to the zone data[4] and the standard DO formulation.[7] The S_4 and S_8 finite element solutions compare very well with the zone method. The same trend is apparent here as demonstrated before[7]; an underprediction in wall flux is reflected by an overprediction in the incident energy near the wall. The FEM solutions satisfy the exact solution,[17] producing an incident energy of unity at $x^* = 0.5$ and $y^* = 0.5$. S_2 solutions produced large errors in the incident energy and are not shown: there was significant overprediction of the incident energy at the hot face and underprediction at the cold face.

Figure 5a shows the predicted net wall heat flux at the center of the lower wall ($x^* = 0.5$ and $y^* = 0$) for the enclosure modeled with various element meshes: 1×1, 2×2, . . . , 10×10. The center value reaches fairly constant values for meshes exceeding 8×8. Figure 5b shows the variation in the net wall heat flux as the S_n approximation is increased. The S_4 approximation provides a reasonable solution without excessive computational effort required by S_6 and S_8 approximations. Solution time depends on the element type, S_n approximation, and the iterations required for convergence:

$$\text{cpu time} \propto c\tfrac{1}{4}n(n+2)i$$

The value c depends on the element type, $c = 1$ for 4 node elements, and ranges 2–3 for 8 node elements. The parameter

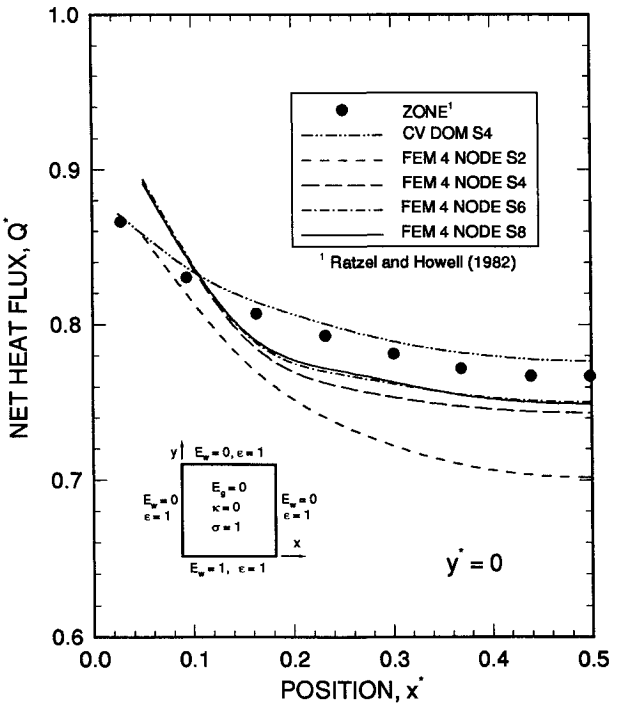

Fig. 3 Net wall heat flux in a square enclosure with scattering medium.

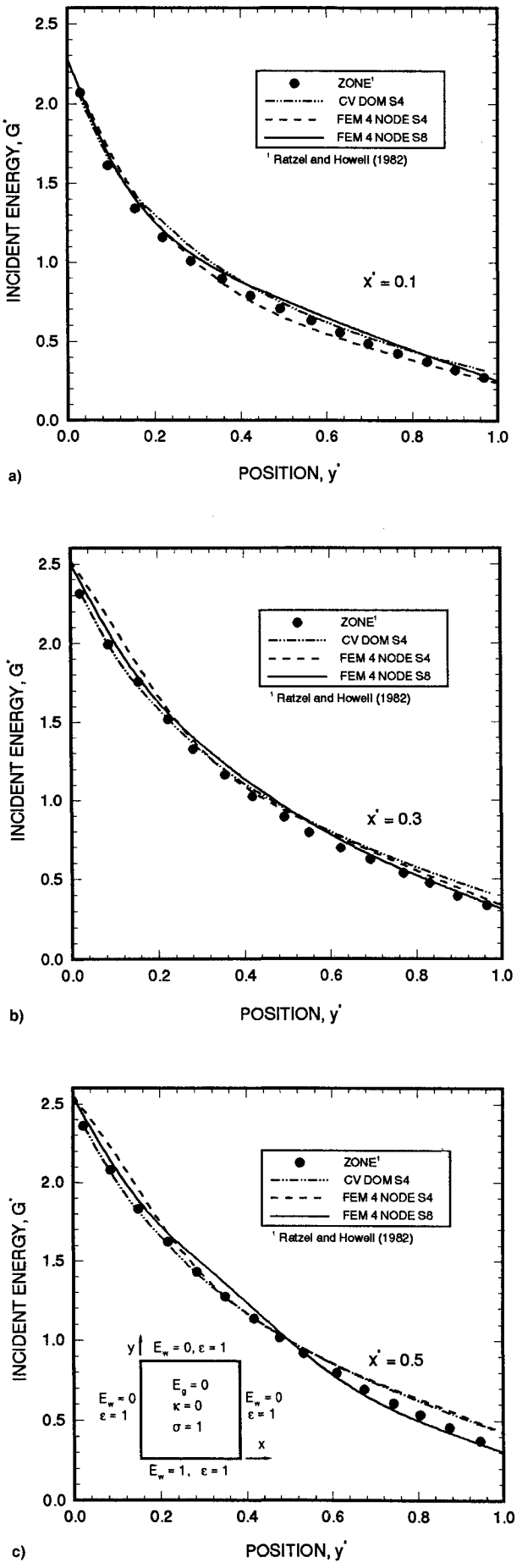

Fig. 4 Incident radiant energy in a square enclosure with scattering medium: a) $x^* = 0.1$, b) $x^* = 0.3$, and c) $x^* = 0.5$.

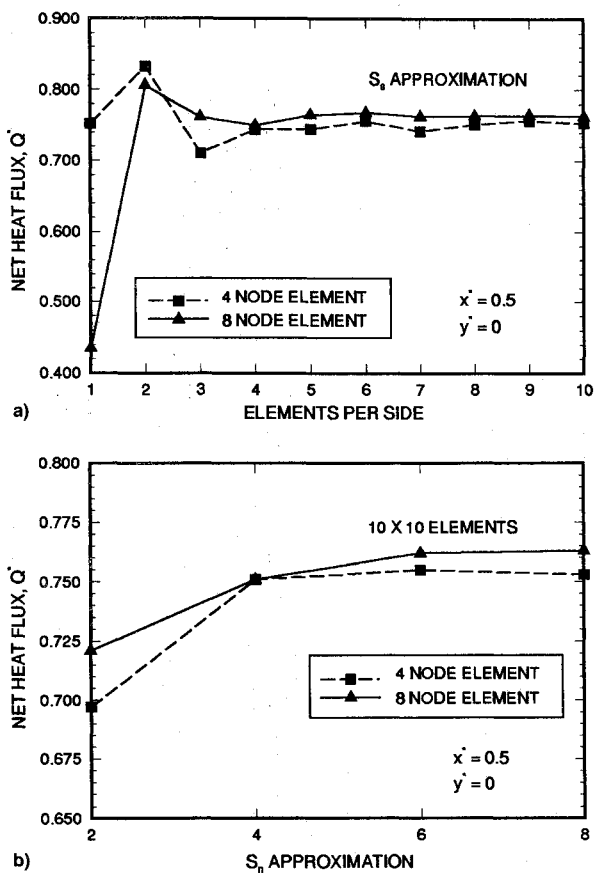

Fig. 5 Convergence of net wall heat flux for scattering medium: a) spatial and b) angular discretization.

n denotes the order of the S_n approximation, and i is the number of iterations required to achieve convergence.

Pure Scattering in a Gray Enclosure

The rectangular enclosure is similar to the previous case, but the walls are assumed radiatively gray with emissivities of 0.5 and 0.1, respectively. This case is important because the boundary conditions are not only a function of the surface emissive power, but the incoming heat flux. Figure 6 shows the predicted net wall heat flux for the FEM S_4 and S_8 solutions, compared to the zone solution and the standard DO solution. At blackbody wall conditions, the wall heat fluxes agree well (within 5%) with the zone and standard DO formulation. As the emissivity is decreased, the predicted fluxes are more uniform and compare well with the zone and standard DO solutions. At an emissivity of 0.1, there is about 15% error between the zone and FEM DO solutions. CPU time increases as the emissivity is decreased: 40–50 iterations were required for the enclosure with an $\varepsilon = 0.5$, while 80–100 are required for the enclosure as ε approaches 0.1. The larger number of iterations is required since the incoming heat flux depends on all of the incoming directions, and is more dominant as $\varepsilon \rightarrow 0$. As emissivity approaches zero, a simultaneous solution of the entire linear system of equations becomes more attractive (see the Solution Methods section).

Black Enclosure with an Absorbing Medium

The finite element method was applied to a rectangular enclosure with cold, black walls and a purely absorbing medium maintained at an emissive power of unity.[7] The geometry was chosen, since an exact solution for heat flux is available.[7,18]

In Fig. 7, the net wall heat flux is predicted for κ of 0.1, 1, and 10 using 4- and 8-node element solutions. Results are shown for several finite element DO solutions compared to the standard DO solution and the exact solution. At an absorption coefficient of 0.1, the S_4 4-node FEM solution overpredicts the centerline heat flux compared to the other solutions and underpredicts the corner fluxes. The 8-node FEM solutions provide a better estimate of the heat flux profile. All solutions compare favorably with the exact solution. At an absorption coefficient of unity, the trend is similar: 8-node elements more accurately capture the heat flux profile. Errors of 1% or less are predicted, which is comparable to the standard DO method. For an absorption index of 10, the 8-node elements resolve the steep gradients near the corners, while the 4-node, linear elements do not. These results are expected because an absorption coefficient of 10 provides a photon mean free path [$\lambda = (1/\kappa)$] on the same order of magnitude as the characteristic element size (for the 10 × 10 discretization). Thus, the errors obtained using the bilinear elements (4 node) were attributed to the inability of a linear profile to capture the exponential nature of the solution within the optical layer close to the boundary surface.

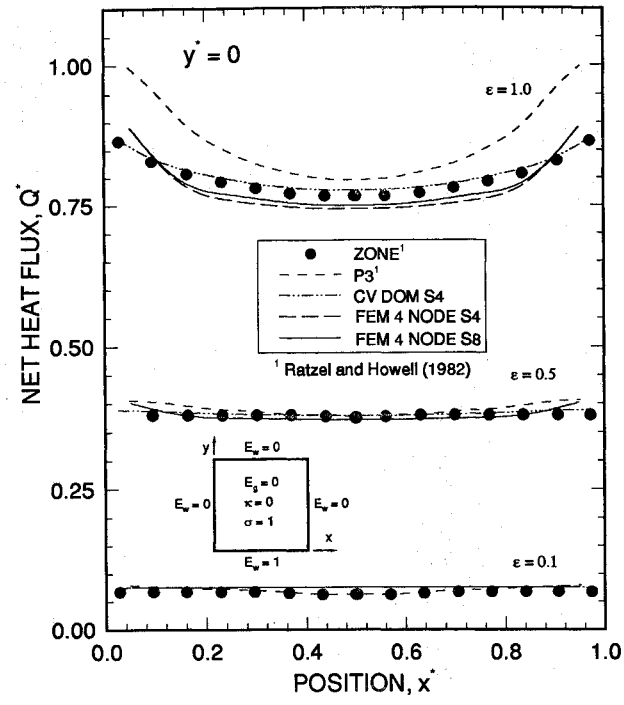

Fig. 6 Net wall heat flux in a gray enclosure with a purely scattering medium.

Figure 8a shows the predicted net wall heat flux at the center line of the lower wall ($x^* = 0.5$ and $y^* = 0$) for the enclosure modeled with various element meshes: 1 × 1, 2 × 2, . . . , 10 × 10. The 8-node FEM values are fairly constant for meshes exceeding 5 × 5. Figure 8b shows the variation in the net wall heat flux as the S_n approximation is increased. There is less than a 2% difference between the S_6 and S_8 solutions.

The strength of the FEM formulation is the capability to treat irregular geometries. To demonstrate this feature, the rectangular enclosure was rotated 30 and 45 deg to produce a rotated rectangle or diamond. The FEM method was used to predict enclosure conditions, and similar results were obtained to those shown in Figs. 7 and 8.

The predictions presented so far were produced using uniformly spaced meshes. To investigate the dependence of the predictions on mesh spacing, several nonuniform meshes were used to predict enclosure net wall heat flux. The meshes were generated using the following relations:

$$\Delta x_i = \alpha \Delta x_{i-1} \qquad i = 2, N_x/2$$

$$\Delta x_i = \Delta x_{N_x - i + 1} \qquad i = N_x/2 + 1, N_x$$

$$\sum_{i=1}^{N_x} \Delta x_i = L$$

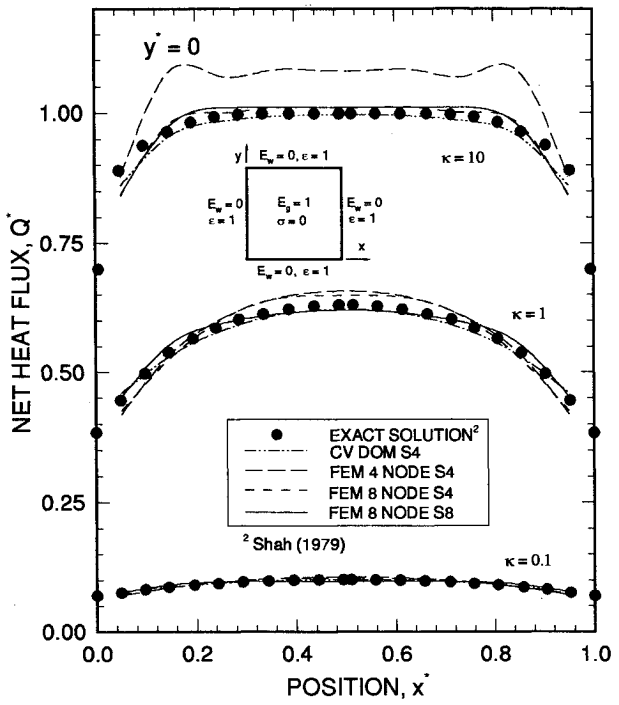

Fig. 7 Net wall heat flux in an enclosure with cold, black walls and a purely absorbing medium.

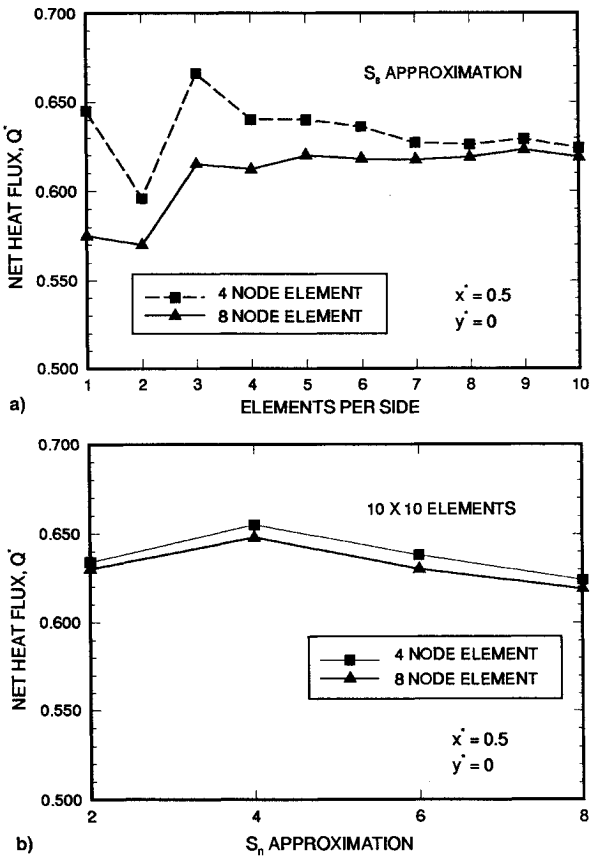

Fig. 8 Convergence of net wall heat flux for absorbing medium: a) spatial and b) angular discretization.

Figure 9a shows a uniform mesh with $\alpha = 1.0$, while Fig. 9d shows a mesh with a doubling of the node-to-node distance. All meshes contain the same number of elements.

Figure 10 shows the predicted net wall heat flux for the control volume discrete ordinates method with a uniform 10 × 10 grid, and for FEM discrete ordinates method with grids

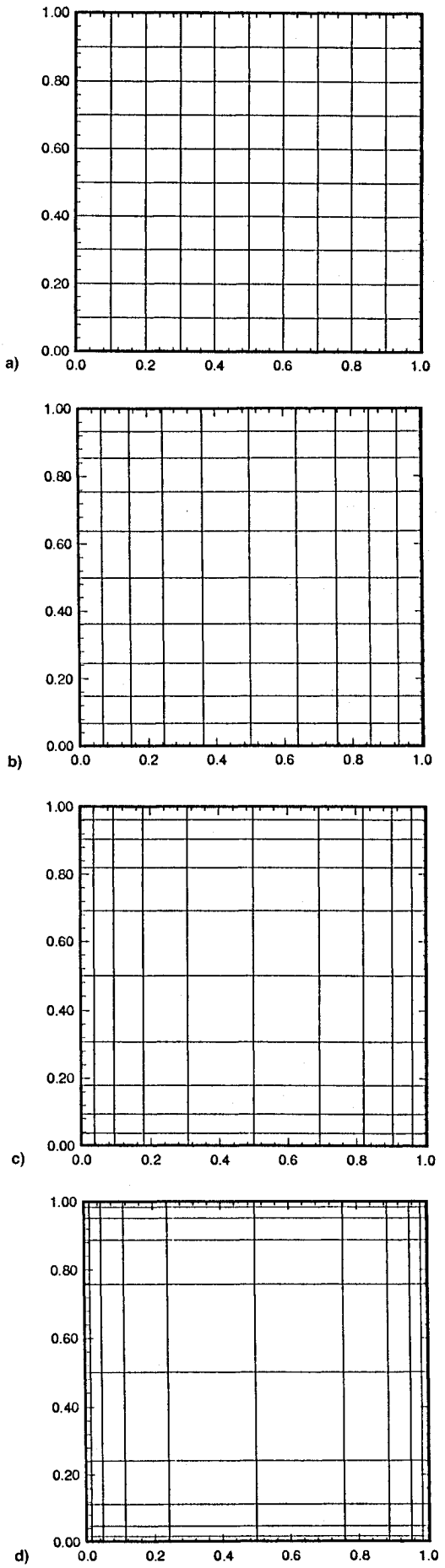

Fig. 9 Nonuniform 10 × 10 meshes a) $\alpha = 1.0$, b) $\alpha = 1.2$, c) $\alpha = 1.5$, and d) $\alpha = 2.0$.

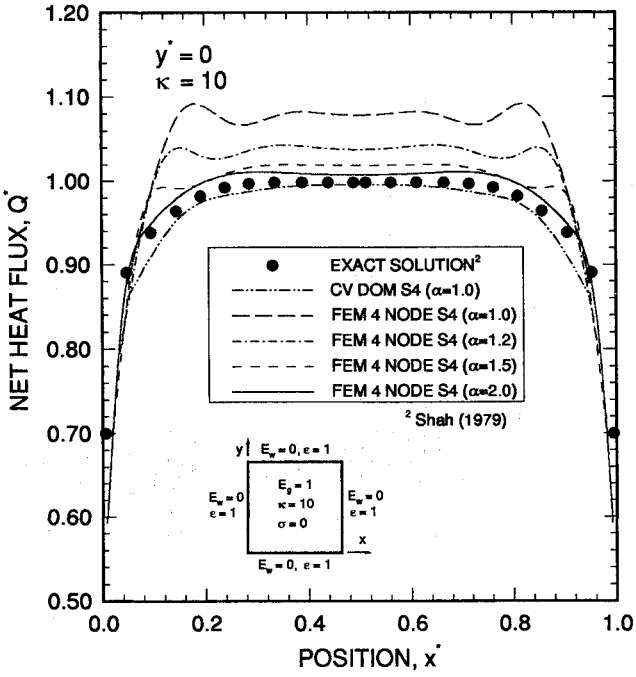

Fig. 10 Variation of net wall heat flux with mesh spacing for a highly absorbing medium.

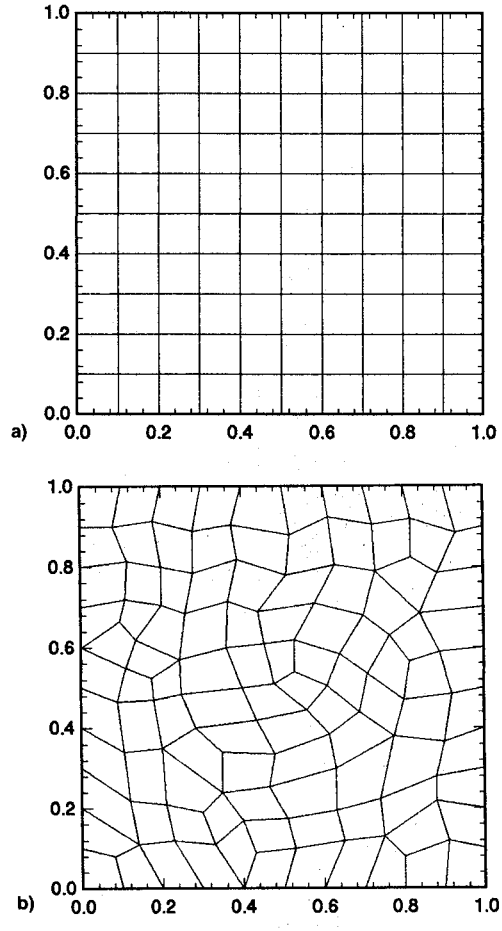

Fig. 11 Structured/unstructured domain discretization a) structured grid and b) unstructured grid.

shown in Fig. 9. An absorption coefficient κ of 10.0—which previously produced anomalous results for 4-node elements—was used for all predictions. The predicted net heat flux on the lower wall varies considerably depending on the grid used. The uniform grid produces values which overpredict the exact solution by 10% at the center and by as much as 15% near

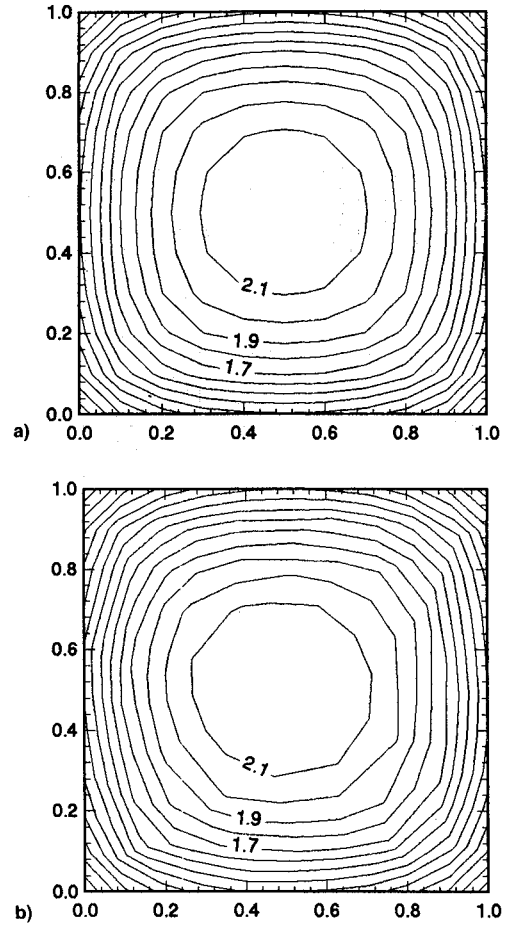

Fig. 12 Incident radiant energy in an enclosure with cold, black walls and a purely absorbing medium a) structured grid and b) unstructured grid.

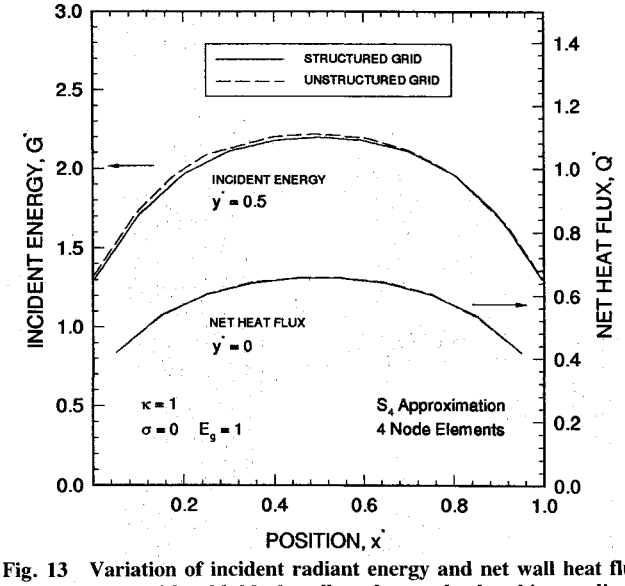

Fig. 13 Variation of incident radiant energy and net wall heat flux in an enclosure with cold, black walls and a purely absorbing medium.

$x = 0$ and $x = 1$. By concentrating elements in regions containing steep gradients, errors are effectively reduced. For the grid with $\alpha = 2.0$, the FEM solution captures all of the features exhibited by the exact solution with errors less than 2%. Further grid refinement may minimize solution error for the given computational effort.

Figure 11 shows structured and unstructured grids for the enclosure with an absorption index of 1.0. Solutions were

found using an S_4 approximation with 4-node elements. In Fig. 12, the predicted incident energy is shown. The incident energy is symmetrical as expected for the structured grid and slightly asymmetric for the unstructured grid. In Fig. 13, the centerline incident energy and heat flux are shown. Excellent agreement was obtained.

Summary

A discrete ordinates method has been presented in this article. This method can be used as an alternative to existing methods for predicting radiative transfer in participating media. The distinct advantage of the formulation and implementation is that solution techniques developed for other transport equations can be used with this method. This includes high-speed solvers for efficient solutions, and adaptive gridding techniques to optimize meshing and minimize solution error.

The FEM DO results for the test cases of pure absorption and scattering compare well with exact solutions and other methods for a range of optical properties and wall emissivities. Solutions indicate the S_4 solution provides solutions with reasonable accuracy without excessive computational time required by the S_6 and S_8 solutions.

More work is needed to test the method for complex geometries, alternative element types, and property variations. This will be necessary to determine where the even parity FEM method best applies compared to other discrete ordinate formulations.

References

[1]Howell, J. R., "Application of Monte Carlo to Heat Transfer Problems," *Advances in Heat Transfer*, Vol. 5, edited by T. F. Irvine Jr. and J. P. Hartnett, Academic Press, New York, 1968, pp. 1–54.

[2]Hottel, H. C., and Sarofim, A. F., *Radiative Transfer*, McGraw-Hill, New York, 1967.

[3]Naraghi, M. H. N., Chung, B. T. F., and Litkouki, B., "A Continuous Exchange Factor Method for Radiative Exchange in Enclosures with Participating Media," *Journal of Heat Transfer*, Vol. 110, No. 2, 1988, pp. 456–462.

[4]Ratzel, A. C., and Howell, J., "Two Dimensional Radiation in Absorbing-Emitting-Scattering Media Using the P-N approximation," American Society of Mechanical Engineers Paper 82-HT-19, 1982.

[5]Menguc, M., and Viskanta, R., "Radiative Transfer in Three-Dimensional Rectangular Enclosures," *Journal of Quantitative Spectroscopy and Radiative Transfer*, Vol. 33, No. 6, 1985, pp. 533–549.

[6]Viskanta, R., and Menguc, M. P., "Radiation Heat Transfer in Combustion Systems," *Prog. Energy Comb. Sci.*, Vol. 13, No. 2, 1987, pp. 97–160.

[7]Fiveland, W. A., "Discrete-Ordinates Solutions of the Radiative Transport Equation for Rectangular Enclosures," *Transactions of ASME, Journal of Heat Transfer*, Vol. 106, 1984, pp. 699–706.

[8]Fiveland, W. A., "Three-Dimensional Radiative Heat Transfer Solutions by the Discrete-Ordinates Method," *Journal of Thermophysics and Heat Transfer*, Vol. 2, No. 4, 1988, pp. 309–316.

[9]Fiveland, W. A., and Jamaluddin, A. S., "Three-Dimensional Spectral Radiative Heat Transfer Solutions by the Discrete Ordinates Method," Vol. 5, No. 3, 1991, pp. 335–339.

[10]Kim, T. K., and Lee, H., "Effect of Anisotropic Scattering on Radiative Heat Transfer in Two-Dimensional Rectangular Enclosures," *International Journal of Heat and Mass Transfer*, Vol. 31, No. 8, 1988, pp. 1711–1721.

[11]Carlson, B. G., and Lathrop, K. D., *Transport Theory—The Method of Discrete-Ordinates in Computing Methods in Reactor Physics*, edited by H. Greenspan, C. Kelber, and D. Okrent, Gordon and Breach, New York, 1968.

[12]Lewis, E. E., and Miller, W. F., *Computational Methods of Neutron Transport*, Wiley, New York, 1984.

[13]Kaplan, S., and Davis, J. A., "Canonical and Involuntary Transformations of the Variational Problems of Transport Theory," *Nuclear Science and Engineering*, Vol. 28, No. 1, 1967, pp. 166–176.

[14]Crandall, S. H., *Engineering Analysis*, McGraw-Hill, New York, 1956.

[15]Zienkiewicz, O. C., and Taylor, R. L., *The Finite Element Method*, Vol. 1, 4th ed., McGraw-Hill, New York, 1989.

[16]Lathrop, K. D., and Carlson, B. G., "Discrete Ordinates Angular Quadrature of the Neutron Transport Equation," Los Alamos Scientific Lab. Rept., LASL-3186, Los Alamos, NM, 1965.

[17]Crosbie, A. I., and Schrenker, R. G., "Exact Expressions for Radiative Transfer in a Three-Dimensional Rectangular Geometry," *Journal of Quantitative Spectroscopy and Radiative Transfer*, Vol. 28, No. 6, 1982, pp. 507–526.

[18]Shah, N., "New Method of Computation of Radiation Heat Transfer in Combustion Chambers," Ph.D. Dissertation, Dept. of Mechanical Engineering, Imperial College of Science and Technology, Univ. of London, London, 1979.